Remote Sensing of Hail with a Dual Linear Polarization Radar

K. AYDIN* AND T. A. SELIGA*

Communications and Space Sciences Laboratory, Department of Electrical Engineering, The Pennsylvania State University, University Park, PA 16802

V. BALAJI*

Advanced Study Program, National Center for Atmospheric Research,† Boulder, CO 80307 and Department of Physics, The Ohio State University, Columbus, OH 43210

(Manuscript received 15 July 1985, in final form 22 April 1986)

ABSTRACT

A technique for the remote sensing of hail with an S-band dual linear polarization radar is described. The method employs a new hail signal H_{DR}, which is derived from disdrometer measurements of raindrop size distributions. Experimental measurements, made in Colorado with the National Center for Atmospheric Research's (NCAR) CP-2 radar system, are used to demonstrate the technique in two major hailstorms.

1. Introduction

Remote sensing of hail within a convective storm remains a challenging goal for radar meteorologists, and various radar hail detection techniques have been proposed to do this since the late 1950s. These include 1) techniques based on reflectivity factor measurements at a single polarization utilizing the intensity of the echo, its structure and time evolution within a storm (Cook, 1958; Douglas and Hitschfeld, 1958; Donaldson, 1961; Geotis, 1963; Donaldson and Burgess, 1982); 2) dual wavelength techniques utilizing the ratio of the reflectivities at 10 and 3 cm wavelengths (Atlas and Ludlam, 1961; Burtsev, 1973; Eccles and Atlas, 1973); and 3) circular polarization techniques based on the measurements of the coherent scattering matrix with a circular polarization radar (Barge, 1972; McCormick and Hendry, 1975). All of these techniques have inherent disadvantages which have limited their utility as an effective means of hail detection (Rinehart and Tuttle, 1982; Bringi et al., 1984b).

In this paper we present a new hail signal based on the differential reflectivity Z_{DR} technique introduced by Seliga and Bringi (1976). Measurements at 10 cm reported by Seliga et al. (1982), Aydin et al. (1984), Leitao and Watson (1984) and Bringi et al. (1984b) with dual linear polarization radars have demonstrated the technique's effectiveness in hail detection. The approach exploits the inherent differences in the radar reflectivities of rain and hail at horizontal and vertical linear polarizations. Observations show that raindrops can be modeled as oblate spheroids with symmetry axes oriented vertically (McCormick et al., 1972; Hendry et al., 1976) and axial ratios dependent on raindrop size (Pruppacher and Beard, 1970; Pruppacher and Pitter, 1971; Bringi et al., 1984a). Therefore, the rain medium appears anisotropic with the principal polarization vectors being closely aligned along the horizontal (H) and vertical (V) directions. In contrast to rain, the hail medium is considered to be significantly more isotropic because hail particles are usually nonspherical and irregularly shaped. Furthermore, experiments and theoretical calculations on the free fall behavior, shape, and internal structure of hailstones (Bailey and Macklin, 1968; Knight and Knight, 1970a,b,c; List et al., 1973; List and Agnew, 1973; Kry and List, 1974a,b; Stewart and List, 1983) indicate that they generally tumble and gyrate, resulting in no preferential orientation. This behavior is consistent with the results of Hendry et al. (1976) and Hendry and Antar (1984), which show that the degree of common alignment of hail is generally much smaller than that of rainfall. There is also a tendency for the reflectivity factor to be greater than 25 dBZ for hail, with the probability of rainfall decreasing as reflectivity increases (Richardson et al., 1983). These properties of hail (isotropy and high reflectivity factor) and rain (anisotropy) are used here as a priori information in defining a new hail signal H_{DR}. Hail detection using this signal was confirmed by ground observations in two major hailstorms in Colorado.

* Previous affiliation: The Atmospheric Sciences Program and Department of Electrical Engineering, The Ohio State University, Columbus, OH 43210.

† The National Center for Atmospheric Research is sponsored by the National Science Foundation.

2. Radar parameters

The reflectivity factor of a volume filled with hydrometeors is defined as

$$Z_{H,V}=\frac{\lambda^4}{\pi^5|K|^2}\int_0^{D_{\max}}\sigma_{H,V}(D)N(D)dD \quad [\text{mm}^6\ \text{m}^{-3}] \quad (1)$$

where $\sigma_{H,V}$ are the backscattering cross sections (mm^2) at horizontal (H) and vertical (V) polarizations, λ is the wavelength (mm), D the equivolume particle diameter (mm) (i.e., the diameter of a sphere having the same volume as the particle), $N(D)$ the particle size distribution ($\text{m}^{-3}\ \text{mm}^{-1}$), $|K| = |m^2 - 1|/|m^2 + 2|$, m being the complex refractive index of the particle, and $|K|^2 = 0.93$ for water at 10 and 3 cm wavelengths (Battan, 1973). In this study all radar measurements, regardless of hydrometeor phase, are assumed to be made employing this same value of $|K|^2$.

The reflectivity factor is usually expressed in dBZ, where 0 dBZ corresponds to 1 $\text{mm}^6\ \text{m}^{-3}$. Differential reflectivity is defined as (Seliga and Bringi, 1976)

$$Z_{DR}(\text{dB}) = 10\log_{10}\frac{Z_H}{Z_V}. \quad (2)$$

In rainfall Z_{DR} is always positive, generally varying between 0 and 4 dB and being correlated with Z_H (and Z_V). In hail Z_{DR} tends to take values around 0 dB compared to larger positive values in the surrounding rain regions, and Z_H (and Z_V) generally increase or maintain a high value in hail regions. This anticorrelated behavior has been used to detect hail in real time by radar with the first ground-based, real-time in situ confirmations reported by Bringi et al. (1984b). In section 3 we use this behavior and the dissimilar backscattering properties of rainfall and hail to define a new hail signal H_{DR} as a simple function of Z_H and Z_{DR}.

3. Raindrop size distributions and radar parameters

An electromechanical disdrometer of the Joss and Waldvogel (1967) type was used to measure drop size distributions in rain. The instrument categorizes drops in 20 size ranges, the smallest one being 0.3 to 0.4 mm and the largest being greater than 5 mm. More details on the operation and calibration of this instrument are also presented in the papers by Waldvogel (1974) and Joss and Waldvogel (1977). Measurements were made in central Illinois and Boulder, Colorado. The difference in the altitudes of these sites have been considered in the evaluation of the data.

Using 2217 drop size distributions, obtained from 2 min running averages of continuous 30 s samples, and the backscattering cross sections for each size category at 10.9 cm wavelength and a temperature of 10°C, the corresponding values of (Z_H, Z_{DR}) were obtained from the discretized forms of (1) and (2). The backscattering cross sections were computed with the T-matrix formulation of Waterman (1969) using raindrop axial ratios obtained from Green's (1975) equation, which closely approximates the measurements of Pruppacher and Pitter (1971). The resulting (Z_H, Z_{DR}) scatter plot is shown in Fig. 1. Note the distinctive upper bound on Z_H, signifying the possibility that measured (Z_H, Z_{DR}) pairs above this boundary could be indicative of hydrometeors other than raindrops. Before considering this possibility, it is important to determine whether the boundary might be associated with limitations on the disdrometer measurements. To do this, computations based on gamma model drop size distributions of the form

$$N(D) = N_m D^m \exp(-\Lambda D) \quad [\text{m}^{-3}\ \text{mm}^{-1}] \quad (3)$$

were performed for different values of N_m, m and $D_{\max}$. These are shown in Fig. 2 and support the presence of an upper bound. Note that the values of the parameters represent both extreme and typical cases of rainfall types (Waldvogel, 1974; Ulbrich, 1983; Goddard and

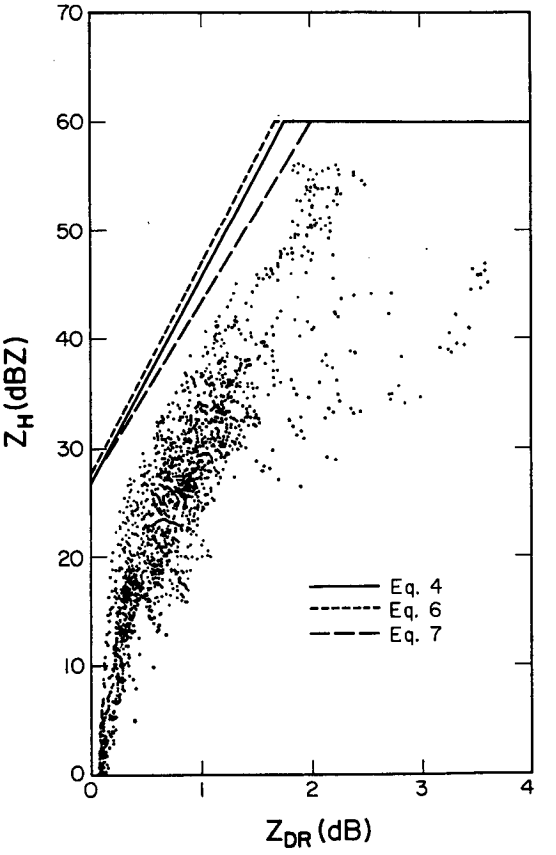

FIG. 1. Reflectivity factor (Z_H) vs differential reflectivity (Z_{DR}) derived from disdrometer measurements of raindrop size distributions. The results are for a wavelength of 10.9 cm and a temperature of 10°C. The 2217 distributions used were obtained in central Illinois and near Boulder, Colorado. The various curves show the rainfall boundaries according to Eqs. (4), (6) and (7).

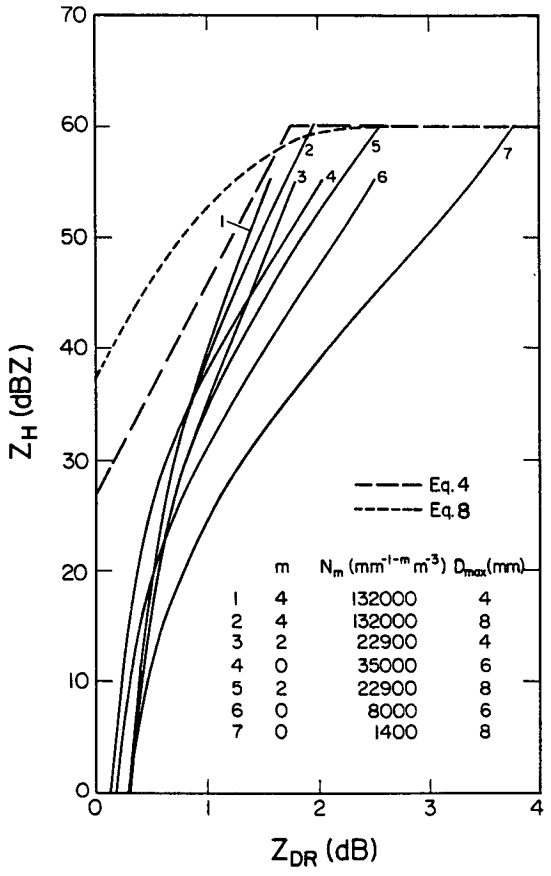

FIG. 2. Reflectivity factor (Z_H) vs differential reflectivity (Z_{DR}) based on model distributions, corresponding to different values of the parameters m, N_m and D_{max} in Eq. (3). Long dashed lines show the rainfall boundary of Eq. (4) and the short dashes the boundary of Eq. (8).

Cherry, 1984). Further confirmation of such an upper bound is also found in measurements reported by Leitao and Watson (1984) obtained with the Chilbolton radar of the Rutherford Appleton Laboratory in England.

A simple parameterization of the inferred rainfall boundary, predicted from disdrometer measurements, is shown in Figs. 1 and 2. An expression for this curve, including truncation at small and high values of Z_{DR} is given by

$$f(Z_{DR}) = \begin{cases} 27, & Z_{DR} \leqslant 0\,(\text{dB}) \\ 19Z_{DR} + 27, & 0 \leqslant Z_{DR} \leqslant 1.74\,(\text{dB}) \\ 60, & Z_{DR} > 1.74\,(\text{dB}). \end{cases} \quad (4)$$

Several features of this equation are worth noting: 1) allowance has been made for the standard errors of the disdrometer data, using estimates of the fractional standard deviations of Z_H and Z_{DR} given in Table 1; 2) allowance has also been made for drop oscillations based on the 50% oscillation model of Seliga et al. (1984); 3) a lower cutoff of $Z_H = 27$ dBZ is chosen for $Z_{DR} \leqslant 0$ dB in order to provide a constant Z_H reference level in this theoretical nonrainfall region; and 4) the upper cutoff of 60 dBZ, although outside the range of the available disdrometer data, is chosen as an upper bound at large Z_{DR}. The latter provides a margin between the upper cutoff and the largest reflectivity factors derived from the disdrometer data. Note that radar measurements by Richardson et al. (1983) indicate the probability of rainfall occurring at $Z_H = 60$ dBZ to be around 0.2. This suggests that the actual upper bound may be even higher (e.g., 65–70 dBZ).

Equation (4) provides a convenient basis for defining a Z_{DR}-derived hail signal:

$$H_{DR} = Z_H - f(Z_{DR}) \quad (5)$$

where Z_H is in dBZ and H_{DR} is in dB. When $H_{DR} > 0$, the radar observables (Z_H, Z_{DR}) lie in the region above (4) in the $Z_H - Z_{DR}$ plane and are taken to signify the presence of hail. Also, the larger H_{DR}, the greater the certainty that the radar reflectivities are not due to raindrops. At low elevation angles below the melting level, H_{DR} should be a good indicator of the presence of hail. Many simultaneous radar and ground-based in situ measurements will be required to assess this scheme. However, recent experiments in Colorado have produced excellent results; two cases from these are presented in section 4 to illustrate these findings.

It is also of interest to determine to what extent drop oscillations affect the rainfall boundary in the $Z_H - Z_{DR}$ plane. Oscillations will tend to decrease Z_{DR} and hence change the boundary. Although ground-based measurements by Jones (1959) show large oscillations of raindrops, there is evidence from aircraft measurements of raindrops (Bringi et al., 1984a) that such severe oscillations are not likely to occur aloft. To determine the effects of moderate and most severe oscillations, the 50% and 100% oscillation models of Seliga et al. (1984) were used. The percentage refers to the maximum oscillation amplitude of raindrops in Jones' (1959) data, which were reexamined by Jameson and Beard (1982), Beard et al. (1983) and Beard (1984). The sampling errors of the disdrometer together with the 50% oscillation model resulted in Eq. (4). Com-

TABLE 1. Estimated fractional standard deviations of reflectivity factor Z_H (mm^6 m^{-3}) and differential reflectivity $Z_{DR} = Z_H/Z_V$ for various rainfall rates R (mm h^{-1}) in thunderstorms. Note that the Z_{DR} used in this table is not in dB.

	R (mm h^{-1})		
Parameter	1	10	100
σ_{Z_H/Z_H}	0.5	0.24	0.12
$\sigma_{Z_{DR}/Z_{DR}}$	0.06	0.03	0.02

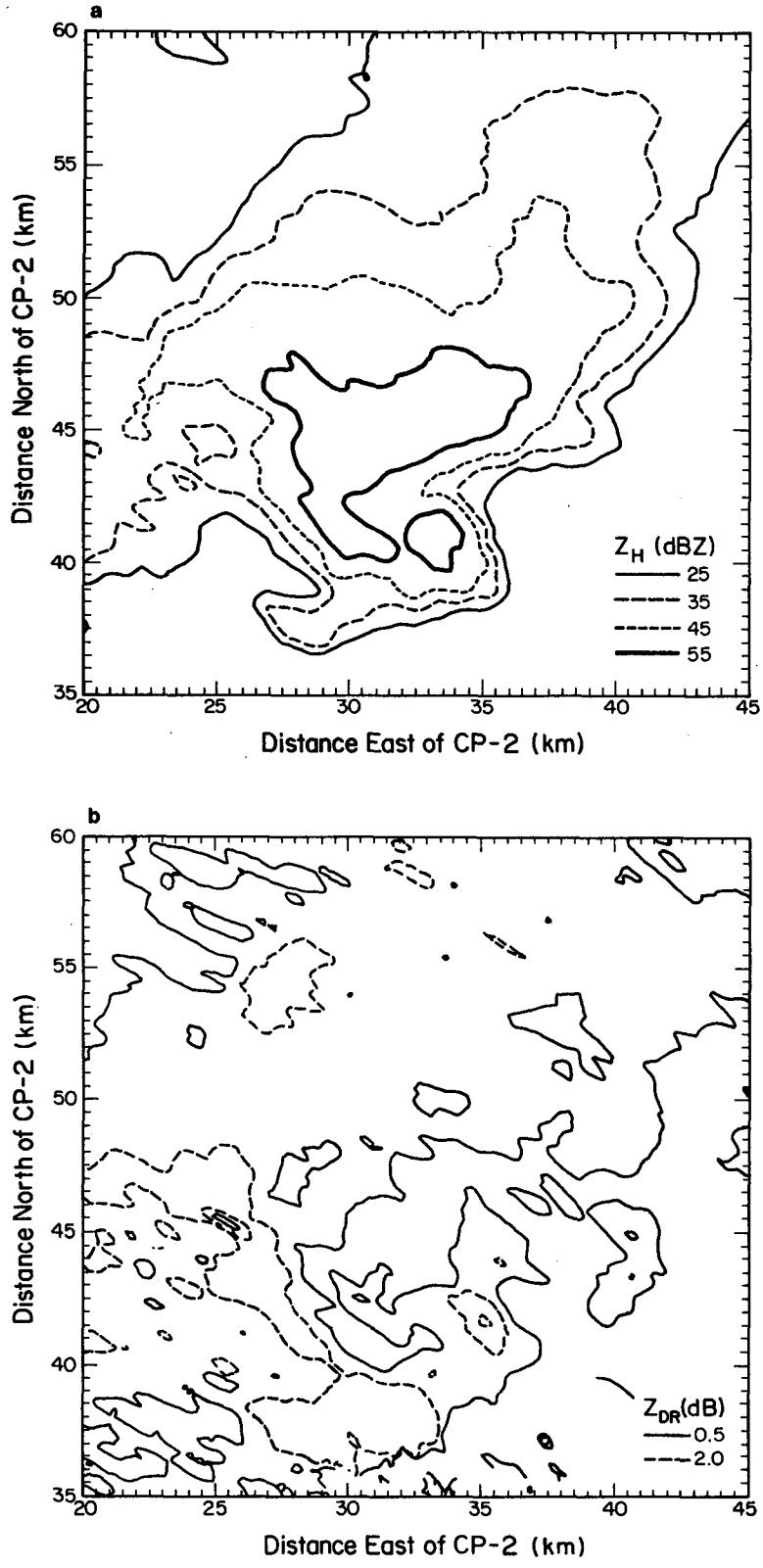

FIG. 3. Contours of (a) Z_H, (b) Z_{DR} and (c) H_{DR} on a constant altitude plane position indicator (CAPPI) scan for a portion of the 4 June 1983 Greeley storm at a height of 400 m above ground. The time of the scan is between 1713:31 and 1715:37 MDT. Hail was reported by ground observers at points A (1712 MDT) and B (1715 MDT; baseball size) in Fig. 3c.

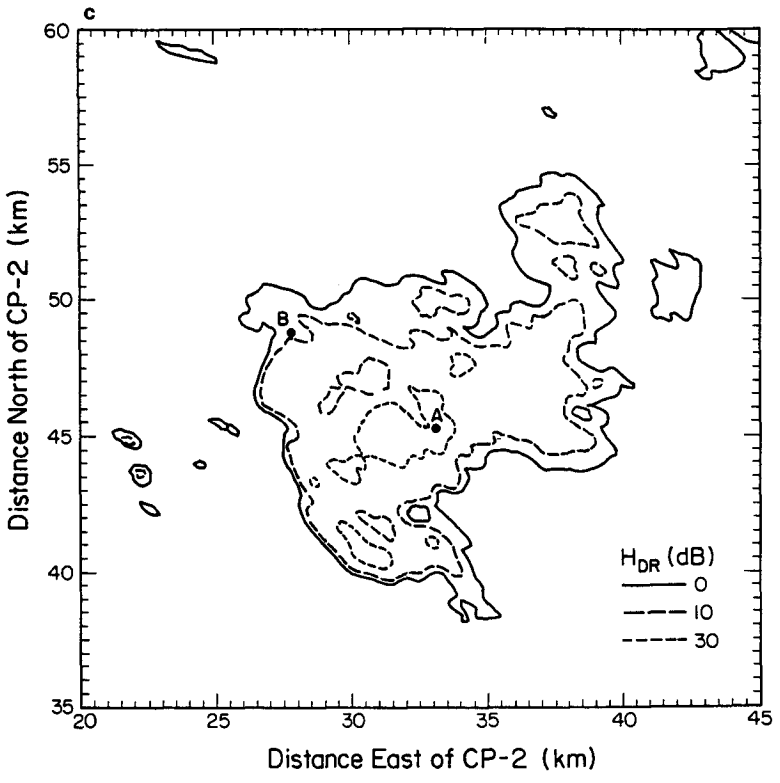

FIG. 3. (*Continued*)

bining the sampling errors with the 100% oscillation model yielded a slightly different expression:

$$f_1(Z_{DR}) = \begin{cases} 27.5, & Z_{DR} \leq 0\,(\text{dB}) \\ 19.5Z_{DR} + 27.5, & 0 \leq Z_{DR} \leq 1.67\,(\text{dB}) \\ 60, & Z_{DR} > 1.67\,(\text{dB}). \end{cases} \quad (6)$$

Excluding oscillations, the rainfall boundary curve reduces to

$$f_0(Z_{DR}) = \begin{cases} 27, & Z_{DR} \leq 0\,(\text{dB}) \\ 16.5Z_{DR} + 27, & 0 \leq Z_{DR} \leq 2\,(\text{dB}) \\ 60, & Z_{DR} > 2\,(\text{dB}). \end{cases} \quad (7)$$

All three boundary curves are plotted in Fig. 1. Note that (6) and (4) differ by around 1.3 dB. The difference between (4) and (7) increases with Z_{DR}, being zero at Z_{DR} = 0 dB and reaching a maximum of 4.3 dB at Z_{DR} = 1.74 dB. In this study the 50% model boundary was considered a reasonable choice for defining H_{DR}. This choice does not appear to be very critical based on radar observations presented in section 4, which show a large spatial gradient of the H_{DR} signal from 0 to 10 dB in regions considered to be hail cells (see Figs. 3c, 4c and 5b). The radar and ground-based in situ observations suggest that the uncertainty of the rainfall boundary in the $Z_H - Z_{DR}$ plane may have only a slight effect on the hail regions detected by H_{DR}. However, it should be stressed that more data of this type are necessary for the statistical assessment of these results.

Prior to examining the Colorado radar observations, consideration of Leitao and Watson's (1984) Chilbolton radar data is of interest, since their upper bound for rainfall lies above the model and disdrometer computations shown in Figs. 1 and 2. Their curve is given by

$$f_{LW}(Z_{DR}) = \begin{cases} -4Z_{DR}^2 + 19Z_{DR} + 37.5, & 0 < Z_{DR} < 2.5\,\text{dB} \\ 60, & Z_{DR} \geq 2.5\,\text{dB} \end{cases} \quad (8)$$

and is generally of the order of 10 dB higher than (4) in the range $0 < Z_{DR} < 0.5$ dB. Above 0.5 dB this difference decreases and becomes zero at Z_{DR} = 1.6 dB.

Several factors may contribute to the difference between the curves. These include possible errors in the radar measurements (Bringi et al., 1983), which are difficult to assess without details of the radar operation.

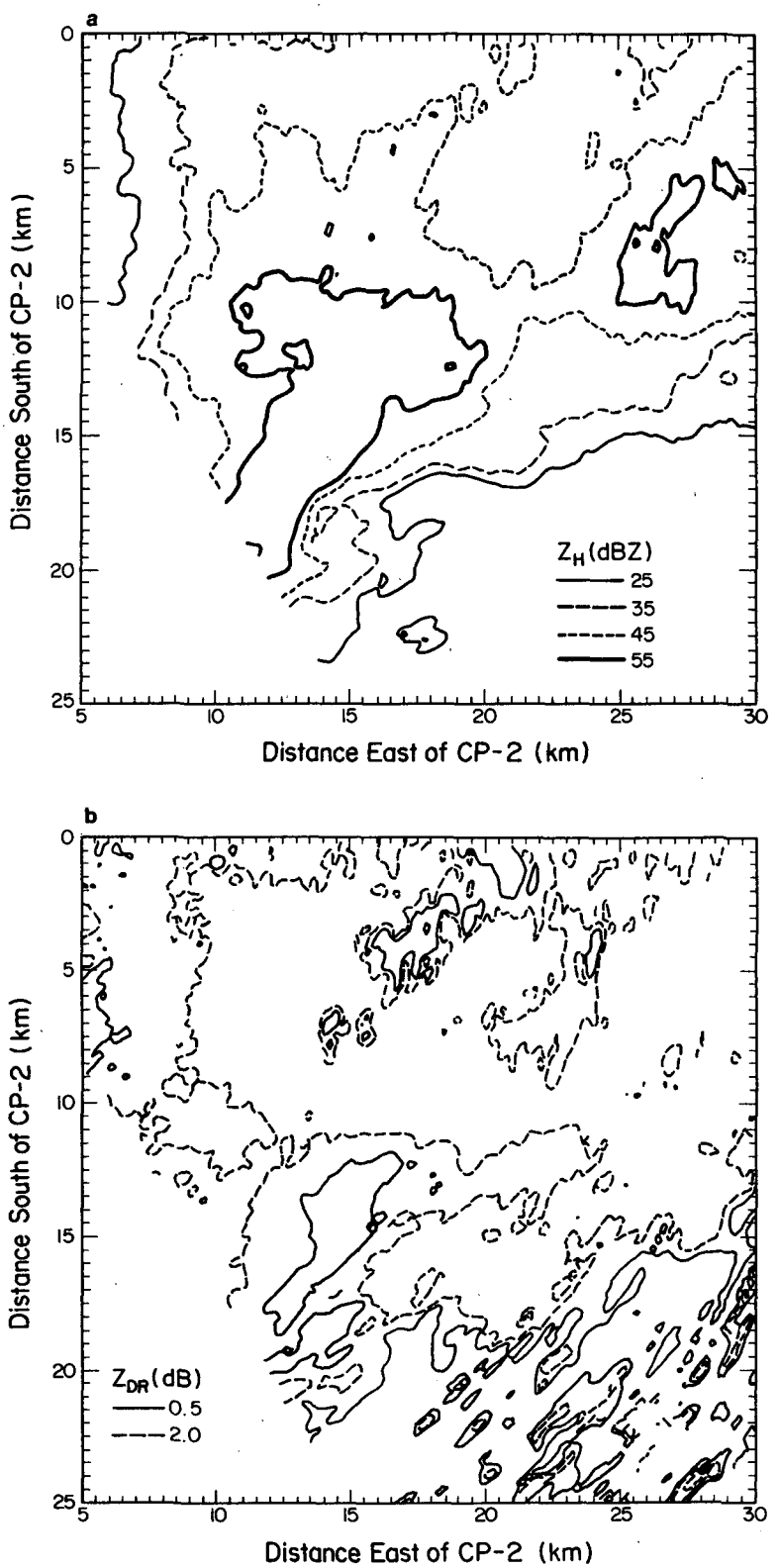

FIG. 4. Contours of (a) Z_H, (b) Z_{DR} and (c) H_{DR} on a constant altitude plan position indicator (CAPPI) scan for a portion of the 13 June 1984 Denver hailstorm at a height of 400 m above ground. The time of the scan is between 1749:34 and 1749:56 MDT. Ground observers reported entering a hail region at 1749 MDT at point A in Fig. 4c and leaving around 13 min later at point B, which is outside the radar scan.

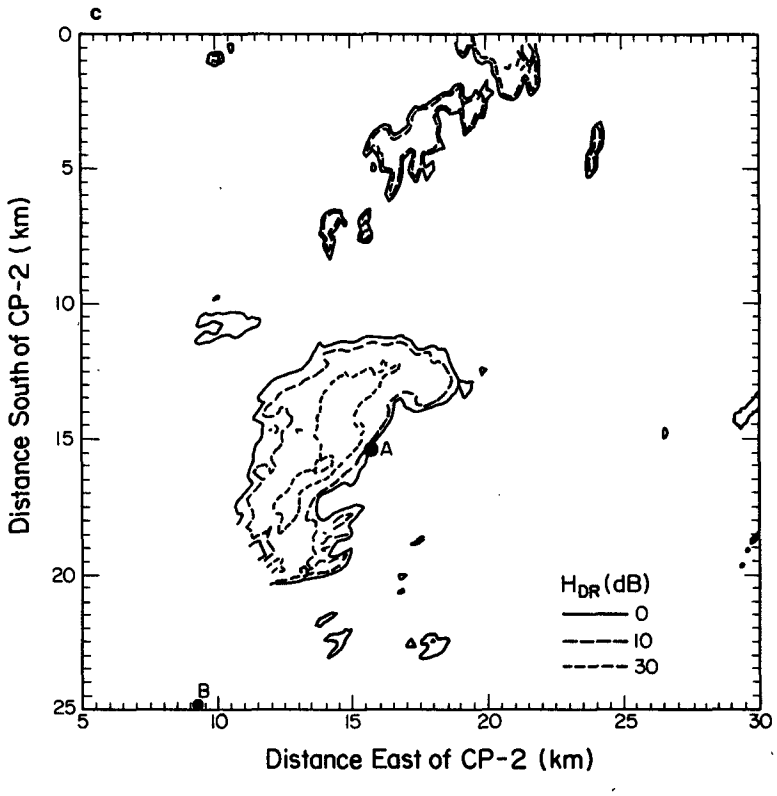

FIG. 4. (*Continued*)

An important factor, helping to explain the discrepancy, may be the significance which Leitao and Watson gave to a very small percentage of radar observations near the edge of their curve. For example, discounting less than 1% of their observations could account for a displacement of their curve downward by as much as 5 dB. Such an effect could easily have been due to observations containing ice phase hydrometeors, since Leitao and Watson's rainfall radar measurements were not confirmed by in situ observations. In contrast, the disdrometer data used to derive H_{DR} in this study were confirmed to be rainfall only by observers at the disdrometer site during the rainfall events. Another factor may be drop oscillations; however, (4) and (6) include the oscillation effects and even for the severe case, (6), the discrepancy persists (see Fig. 1). Other possible contributing factors to the discrepancy may be attributed to the different meteorological regimes in which the data were obtained. The Chilbolton radar is in a maritime regime, while the disdrometer measurements were made in a continental regime. Maritime rainfall is often characterized by the presence of large numbers of very small raindrops (e.g., see Ugai et al., 1977) compared to continental rainfall.

Ultimately, the final choice of curve for the rainfall boundary in the $Z_H - Z_{DR}$ plane from which a hail signal such as H_{DR} may be defined will depend on in situ verification of many radar observations under varying circumstances and in different geographical areas. The results in section 4 illustrate the application of the scheme.

4. Radar observations

The two storms reported here were observed using the National Center for Atmospheric Research's (NCAR) CP-2 radar system during project MAYPOLE (May Polarization Experiment). This project was a collaborative research program of The Ohio State University, Colorado State University, and NCAR to evaluate the performance of the CP-2 as a multiparameter radar.

The first convective storm to be considered passed over Greeley, Colorado, on 4 June 1983. The radar was located at the Eastlake site, approximately 50–55 km south-southwest of Greeley. Mobile chase teams of the Prototype Regional Observing and Forecasting System (PROFS) of the National Oceanic and Atmospheric Administration (NOAA) were in the area providing in situ ground-level observations. The second storm occurred on 13 June 1984 in the vicinity of Denver, Colorado. In this case the CP-2 radar was at the Marshall site, located approximately 10 km southeast of Boulder. Mobile teams of the Convective Storms Division (CSD)

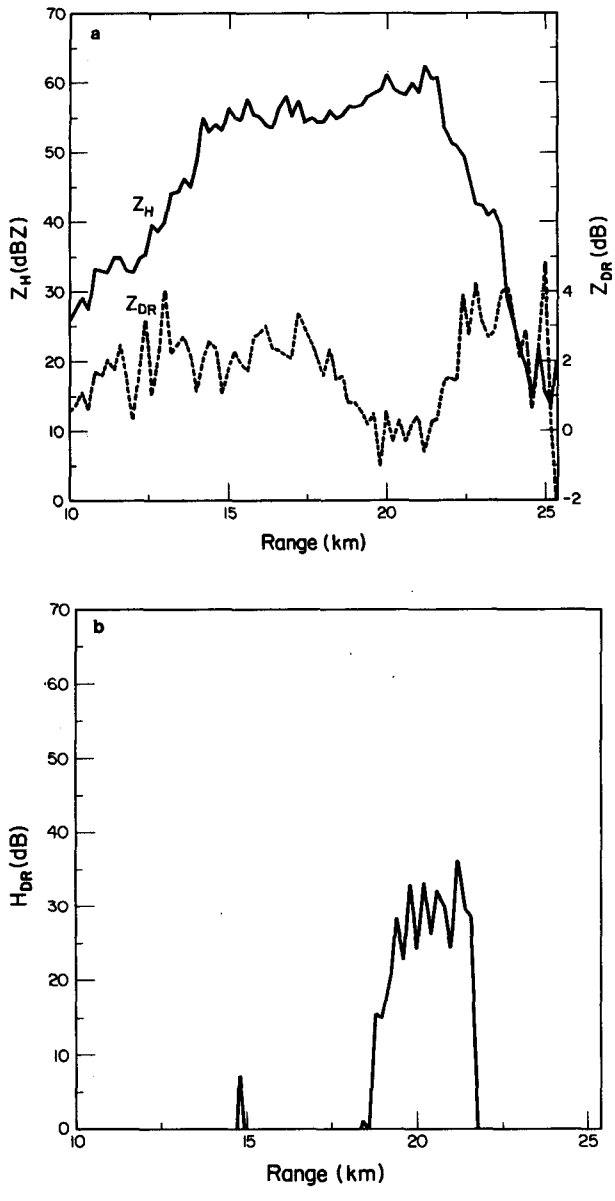

FIG. 5. Fields of (a) Z_H and Z_{DR} and (b) H_{DR} along a portion of a ray through point A of Fig. 4c at the lowest elevation angle (0.4°) scan. Point A is 22 km from the radar along this ray (135° azimuth). The time is 1749:52 MDT.

and the Field Observing Facility (FOF) of NCAR were in the area and in radio contact with the radar, whence the radar operators were able to guide the teams toward hail regions, using the real-time hail detection capability made possible by (Z_H, Z_{DR}) measurements. Numerous independent reports of hail and damage are also available for both the Greeley and Denver storms in NOAA's Storm Data (1983, 1984) and local newspaper reports.

Figure 3 shows contours of Z_H, Z_{DR}, and H_{DR}, computed from (4), on a constant altitude plan position indicator (CAPPI) scan through the Greeley storm. Hail reports from the PROFS mobile teams were received from the points marked A and B around the time of the scan. (See the caption of Fig. 3.) Figure 4 shows the same fields contoured for the Denver hailstorm. At the time of this scan the CSD hail chase team reported entering a hailswath at point A and leaving it around 13 min later at point B. It is worth noting that the 0 and 10 dB contours of the hail signal are very closely spaced in Figs. 3c and 4c and, therefore, define the hail region well. The sharpness of the transition is even more apparent in Fig. 5, which shows plots of the fields on a single ray through the point A in Fig. 4. It is presumed that this sharp gradient signals a change from dominance by rainfall to hail in the microphysical constitution of the volume being sampled by the radar.

The general features of the H_{DR} contour plots in Figs. 3c and 4c are also interesting. They indicate an apparent intensity of hail which is correlated with reflectivity factor and which, in the more intense regions, signifies a greater certainty that the hydrometeor backscatter is from precipitation other than rainfall. If the greater Z_H is associated with more and larger hailstones, then H_{DR} or similarly defined hail signals may yield a very good measure of hailfall kinetic energy. This hypothesis will require much future testing of the type performed, for example, by Waldvogel et al. (1978b) and Waldvogel and Schmidt (1982), who compared hail pad estimates of kinetic energy with radar-derived values using 55 dBZ as a threshold criteria for hail detection.

It is of interest to compare the 55 dBZ threshold criterion with H_{DR}. The Z_H contours in Fig. 3a were selected to show the 55 dBZ level. The Greeley results show two ground-based hail observations of the PROFS chase team inside the H_{DR} contour. One of these locations lies inside the 55 dBZ contour and the other is just outside of it. In this case the H_{DR}-detected hail region is about twice the area of the 55 dBZ contour region, although all of the latter resides within the H_{DR} contour.

The Denver storm (Figs. 4a, c) exhibited somewhat different behavior in that the 55 dBZ contoured regions extend over considerably larger areas than the H_{DR} regions. The comparisons show an extended region with large H_{DR} signals (>10 dB) around 17 km east and 4 km south, where Z_H is less than 55 dBZ. In this case NOAA's Storm Data (1984) reported golfball size hail occurring at 1634 MST (i.e., 1734 MDT, 15 min before the scan) in Westminster, which lies just south-southwest of this region where the two strong, small, isolated H_{DR} cells occur. The storm track was north-northeasterly. In contrast to this observation, Storm Data reported no hail around the time of the scan near the isolated 55 dBZ contoured region at 26 km east and 8 km south, which is just east of Thornton.

Figure 6 shows a scatter plot of Z_H versus Z_{DR} used in obtaining the CAPPI contour plots of Fig. 4 for the Denver hailstorm. The solid line is the rainfall boundary as given by Eq. (4). There is a clustering of points below and to the right of this boundary which are pre-

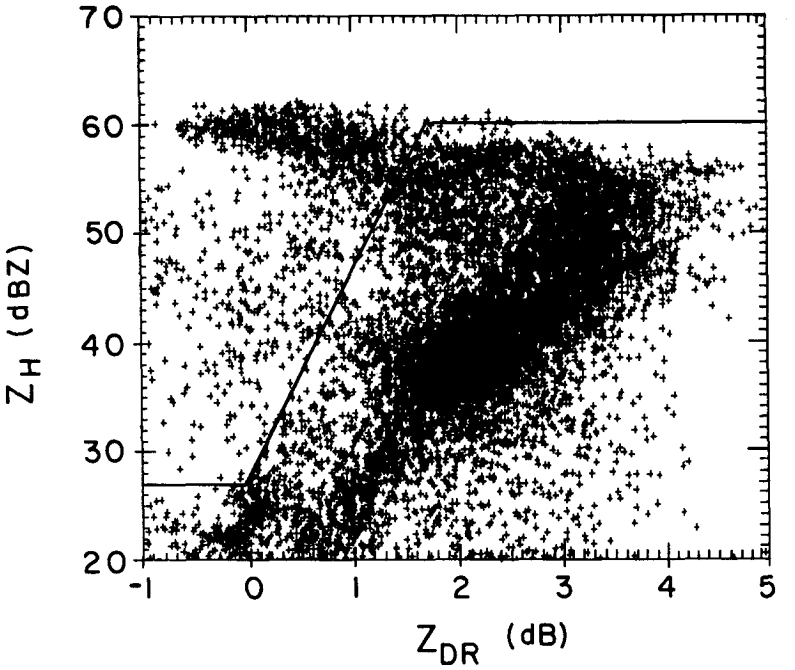

FIG. 6. Scatter plot of Z_H vs Z_{DR} from the radar CAPPI data shown in Fig. 4a, b. The solid line is the rainfall boundary of Eq. (4).

sumed to be mainly from rain, and possibly some points other than rain (e.g., ground clutter). The cluster of points above and to the left of the rainfall boundary are expected to be dominantly from hail. There is also a transition region around $Z_H = 55$ dBZ and $Z_{DR} = 1.5$ dB. Radar measurements together with in situ or ground-based observations are necessary for better understanding of this transition region. It should also be noted that in order for any of these data to be meaningful they should produce a spatially continuous picture as shown by the contours in Fig. 4.

5. Conclusions

The remote sensing of hail by a dual linear polarization (differential reflectivity) radar was demonstrated by using a new hail signal H_{DR}. H_{DR} was derived from differences in the radar reflectivities of rain and hail at horizontal and vertical linear polarizations. Disdrometer measurements of raindrop size distributions and model gamma distributions fell within a well-defined region of the Z_H–Z_{DR} plane. The (Z_H, Z_{DR}) pairs lying above the boundary of the rainfall region were considered to represent hail and were used as the basis for defining H_{DR}.

H_{DR} contours in two major hail storms in Colorado exhibited strong gradients at the edges of the hail regions and a wide dynamic range. In situ observations of hail by mobile chase teams and comparison with Storm Data reports all gave positive confirmations of H_{DR} as a hail signal. On the other hand, 55 dBZ reflectivity factor threshold levels were also generally indicative of hail regions based on ground confirmations. However, in a CAPPI from the Greeley hailstorm the positive H_{DR} hail signal region was about twice the area of the 55 dBZ contour region which resided within the H_{DR} contour. Conversely, in a CAPPI from the Denver hailstorm the 55 dBZ contoured regions extended over larger areas than the H_{DR} regions. Thus, the 55 dBZ reflectively factor threshold did not always agree with H_{DR}.

Although this study and others under way in the MAYPOLE experiments are highly supportive of the H_{DR} hail detection technique, many more studies are required to gain statistical confidence in its interpretations. Of particular importance will be detailed ground-based observations with extensive areal coverage to determine exactly how well H_{DR} defines hail regions, what the influence of mixed phase (rain and hail) is on H_{DR}, and whether H_{DR} may be utilized for kinetic energy estimation of hailfall.

Acknowledgments. This work was supported by the Atmospheric Research Section, National Science Foundation under Grant ATM-8003376 and by the Army Research Office through the University Corporation for Atmospheric Research under Subcontract NCAR S3025. We are grateful to R. E. Carbone, P. H. Herzegh and other staff members of the Field Observing Facility of NCAR and to V. N. Bringi of the Colorado State University for their collaboration during project MAYPOLE. The cooperation of the mobile chase teams, provided by NCAR's CSD and NOAA's PROFS, is also gratefully acknowledged. Software sup-

port for radar data analysis was provided by C. Mohr and L. J. Miller of NCAR's CSD. NCAR is supported by the National Science Foundation.

REFERENCES

Atlas, D., and F. H. Ludlam, 1961: Multi-wavelength radar reflectivity of hailstorms. *Quart. J. Roy. Meteor. Soc.*, **87,** 523–534.

Aydin, K., T. A. Seliga and V. N. Bringi, 1984: Differential radar scattering properties of model hail and mixed-phase hydrometeors. *Radio Sci.*, **19,** 58–66.

Bailey, I. H., and W. C. Macklin, 1968: The surface configuration and internal structure of artificial hailstones. *Quart. J. Roy. Meteor. Soc.*, **94,** 1–11.

Barge, B. L., 1972: Hail detection with a polarization diversity radar. Sci. Rep. MW-71, Stormy Weather Group, McGill University, 80 pp.

Battan, L. J., 1973: *Radar Observations of the Atmosphere,* The University of Chicago Press, 324 pp.

Beard, K. V., 1984: Oscillation models for predicting raindrop axis and backscatter ratios. *Radio Sci.*, **19,** 67–74.

——, D. B. Johnson and A. R. Jameson, 1983: Collisional forcing of raindrop oscillations. *J. Atmos. Sci.*, **40,** 455–462.

Bringi, V. N., T. A. Seliga and S. M. Cherry, 1983: Statistical properties of the dual-polarization differential reflectivity (Z_{DR}) hail signal. *IEEE Trans. Geosci. Remote Sensing,* **21,** 215–220.

——, —— and W. A. Cooper, 1984a: Analysis of aircraft hydrometeor spectra and differential reflectivity (Z_{DR}) radar measurements during the Cooperative Convective Precipitation Experiment. *Radio Sci.*, **19,** 157–167.

——, —— and K. Aydin, 1984b: Hail detection with a differential reflectivity radar. *Science,* **225,** 1145–1157.

Burtsev, I. I., 1973: *Modification of Hail Processes.* Gidrometeorizdat Publ., 241 pp. [Available from the U.S. Dept. of Commerce, NTIS.]

Cook, B., 1958: Hail determination by radar analysis. *Mon. Wea. Rev.*, **86,** 435–438.

Donaldson, R. J., Jr., 1961: Radar reflectivity profiles in thunderstorms. *J. Meteor.*, **18,** 292–305.

——, and D. W. Burgess, 1982: Results of the Joint Doppler Operational Project. *Proc. NEXRAD Doppler Radar Symp./Workshop,* University of Oklahoma (Norman), NOAA, 102–123.

Douglas, R. H., and W. Hitschfeld, 1958: Studies of Alberta hailstorms, 1957. Sci. Rep. MW-27, Stormy Weather Group, McGill University, 79 pp.

Eccles, P. J., and D. Atlas, 1973: A dual-wavelength radar hail detector. *J. Appl. Meteor.*, **12,** 847–854.

Geotis, S. G., 1963: Some radar measurements of hailstorms. *J. Appl. Meteor.*, **2,** 270–275.

Goddard, J. W. F., and S. M. Cherry, 1984: Quantitative precipitation measurements with dual linear polarization radar. *Preprints 21st Conf. on Radar Meteor.,* Edmonton, Amer. Meteor. Soc., 352–357.

Green, A. W., 1975: An approximation for the shapes of large raindrops. *J. Appl. Meteor.*, **14,** 1578–1583.

Hendry, A., and Y. N. M. Antar, 1984: Precipitation particle identification with centimeter wavelength dual-polarization radars. *Radio Sci.*, **19,** 115–122.

——, G. C. McCormick and B. L. Barge, 1976: The degree of common orientation of hydrometeors observed by polarization diversity radars. *J. Appl. Meteor.*, **15,** 635–640.

Jameson, A. R., and K. V. Beard, 1982: Raindrop axial ratios. *J. Appl. Meteor.*, **21,** 257–259.

Jones, D. M. A., 1959: The shape of raindrops. *J. Atmos. Sci.*, **16,** 504–510.

Joss, J., and A. Waldvogel, 1967: Ein Spektrograh fur Niederschlagstropher mit automatischer Auswertung. *J. Pure Appl. Geophys.*, **68,** 240–246.

——, and ——, 1977: Comments on "Some observations on the Joss–Waldvogel Rainfall Disdrometer." *J. Appl. Meteor.*, **16,** 112–113.

Knight, C. A., and N. C. Knight, 1970a: Hailstone embryos. *J. Atmos. Sci.*, **27,** 659–666.

——, and ——, 1970b: Lobe structures of hailstones. *J. Atmos. Sci.*, **27,** 667–671.

——, and ——, 1970c: Falling behavior of hailstones. *J. Atmos. Sci.*, **27,** 672–681.

Kry, P. R., and R. List, 1974a: Aerodynamic torques on rotating oblate spheroids. *Phys. Fluids,* **17,** 1087–1092.

——, and ——, 1974b: Angular motions of freely falling spheroidal hailstone models. *Phys. Fluids,* **17,** 1093–1102.

Leitao, M. J., and P. A. Watson, 1984: Application of dual linearly polarized radar data to prediction of microwave path attenuation at 10–30 GHz. *Radio Sci.*, **19,** 209–221.

List, R., and T. A. Agnew, 1973: Air bubbles in artificial hailstones. *J. Atmos. Sci.*, **30,** 1158–1165.

——, U. W. Rentsch, A. C. Bayram and E. P. Lozowski, 1973: On the aerodynamics of spheroidal hailstone models. *J. Atmos. Sci.*, **30,** 653–661.

McCormick, G. C., and A. Hendry, 1975: Principles for the radar determination of the polarization properties of precipitation. *Radio Sci.,* 421–434.

——, —— and B. L. Barge, 1972: The anisotropy of precipitation media. *Nature,* **238,** 214–216.

NOAA, 1983: *Storm Data.* 25(6), Publications Section (E/cc413), Nat. Climatic Data Center, NOAA/NESDIS, 11–12.

——, 1984: *Storm Data.* 26(6), Publications Section (E/cc413), Nat. Climatic Data Center, NOAA/NESDIS, 24.

Pruppacher, H. R., and K. V. Beard, 1970: A wind tunnel investigation of the internal circulation and the shape of water drops falling at terminal velocity in air. *Quart. J. Roy. Meteor. Soc.*, **96,** 247–256.

——, and R. L. Pitter, 1971: A semi-empirical determination of the shape of the cloud and raindrops. *J. Atmos. Sci.*, **28,** 86–94.

Richardson, S., B. L. Barge and R. G. Humphries, 1983: Hailfall probability based on radar reflectivity. *Preprints 21st Conf. on Radar Meteor.,* Edmonton, Amer. Meteor. Soc., 421–424.

Rinehart, R. E., and J. D. Tuttle, 1982: Antenna beam patterns and dual-wavelength processing. *J. Appl. Meteor.*, **21,** 1865–1880.

Seliga, T. A., and V. N. Bringi, 1976: Potential use of radar reflectivity measurements at orthogonal polarizations for measuring precipitation. *J. Appl. Meteor.*, **15,** 69–76.

——, K. Aydin, C. P. Cato and V. N. Bringi, 1982: Use of radar differential reflectivity technique for observing convective systems. *Cloud Dynamics,* Reidel, 285–300.

——, ——, and V. N. Bringi, 1984: Differential reflectivity and circular depolarization ratio radar signals and related drop oscillation and propagation effects in rainfall. *Radio Sci.*, **19,** 81–89.

Stewart, R. E., and R. List, 1983: Gyrational motion of disks during free-fall. *Phys. Fluids,* **26,** 920–927.

Ugai, S., K. Kato, M. Nishijima, T. Kan and K. Tazaki, 1977: Fine structure of rainfall. *Ann. Telecomm.*, **32,** 421–429.

Ulbrich, C. W., 1983: An empirical method for accounting for variations in the form of the raindrop size measurements in dual-measurement techniques. *Preprints 21st Conf. on Radar Meteor.,* Edmonton, Amer. Meteor. Soc., 317–322.

Waldvogel, A., 1974: The N_0 jump of raindrop spectra. *J. Atmos. Sci.*, **31,** 1067–1078.

——, and W. Schmid, 1982: The kinetic energy of hailfalls, part III: Sampling errors inferred from radar data. *J. Appl. Meteor.*, **21,** 1228–1238.

——, —— and B. Federer, 1978a: The kinetic energy of hailfalls, part I: Hailstone spectra. *J. Appl. Meteor.*, **17,** 515–520.

——, —— and ——, 1978b: The kinetic energy of hailfalls, part II: Radar and hailpads. *J. Appl. Meteor.*, **17,** 1683–1690.

Waterman, P. C., 1969: Scattering by dielectric obstacles. *Alta Freq.*, **38,** 348–352.